# Facile synthesis of α-$Fe_2O_3$ micro-ellipsoids by surfactant-free hydrothermal method for sub-ppm level $H_2S$ detection

Zhijie Li[1], Zhijie Lin[1], Ningning Wang[1], Yanwu Huang[1], Junqiang Wang[1], Wei Liu[1],

Yongqing Fu[1,2*], Zhiguo Wang[1*]

[1]School of Physical Electronics, University of Electronic Science and Technology of China, Chengdu 610054, PR China

[2]Department of Physics and Electrical Engineering, Faculty of Engineering and Environment, Northumbria University, Newcastle Upon Tyne NE1 8ST, England, United Kingdom

**Abstract**

The α-$Fe_2O_3$ micro-ellipsoids were prepared using a facile hydrothermal process without any surfactant or template, and their morphological, structural and $H_2S$ sensing properties were investigated. The α-$Fe_2O_3$ showed uniform micro-ellipsoids with a long axis diameter of 1.7 μm and a short axis diameter of 1.2 μm. Detailed structural analysis confirmed that the synthesized α-$Fe_2O_3$ micro-ellipsoids were compact particles with a hexagonal structure. Gas sensor base on the α-$Fe_2O_3$ micro-ellipsoids showed excellent response, short response/recovery time (less than 90 s and 30 s, respectively), low detection concentration (~0.5 ppm), good long-term stability and excellent selectivity towards $H_2S$ gas at the optimized operating temperature of 350 $^oC$. The sensing mechanism of the sensor based on the α-$Fe_2O_3$ micro-ellipsoids towards $H_2S$ was discussed.

**Keywords:** α-$Fe_2O_3$; Micro-ellipsoid; Hydrothermal; $H_2S$; Gas sensor

---

* Corresponding author. Tel.: +86 02883200728. E-mail address: zgwang@uestc.edu.cn (Zhiguo Wang); Richard.fu@northumbria.ac.uk (Yongqing Fu)

## 1. Introduction

Hematite ($\alpha$-$Fe_2O_3$) is one of the n-type metal oxide semiconductor materials widely utilized in the fields of catalysts, waste water treatment, pigment, magnetic materials, photo-catalyst, and electrode materials in lithium ion batteries [1-7]. Specially, $\alpha$-$Fe_2O_3$ is believed to be a promising sensing material due to its nontoxicity, stability and low cost. Various $Fe_2O_3$ nanostructures have been synthesized and applied for the detection of CO [8], $H_2S$ [9], $NO_2$ [10], hydrocarbon gases [11-13] and alcohol [14]. For example, Bandgar et al [15] reported that hybrid nanocomposites films with $\alpha$-$Fe_2O_3$ nanoparticles were highly selective to $NH_3$ with good response (50 at 100 ppm), fast response time (29 s) and highly reproducible response curves. Bandgar et al [16] and Navale et al [17] fabricated $\alpha$-$Fe_2O_3$ thin film sensor on glass substrate using the sol–gel spin coating technique, and the sensors showed a good response (17%) for $NO_2$ gas at 200 $^oC$. Han et al [18] reported that liquefied petroleum gas (LPG) sensors with hematite nanoparticles-chains showed a superior sensitivity.

Many $\alpha$-$Fe_2O_3$ nanostructures with various morphologies have been synthesized, including nanowires [19], nanorods [20,21], nanobelt [22], nanofiber [23,24], nanospheres [25], nanotubes [26-28] and porous $\alpha$-$Fe_2O_3$ [29, 30]. However, it is still a big challenge to find a facile preparation technique for the $\alpha$-$Fe_2O_3$ with special morphologies in order to achieve excellent gas sensing properties, such as good response, short response/recovery time, good long-term stability and selectivity. Especially there are no reports to fabricate the $H_2S$ gas sensor using the $\alpha$-$Fe_2O_3$ micro-ellipsoids, which should be stable than $\alpha$-$Fe_2O_3$ nanostructures in applications.

In this work, the $\alpha$-$Fe_2O_3$ micro-ellipsoids were synthesized using a one-step hydrothermal method without any surfactant or template. Gas sensors based on the $\alpha$-$Fe_2O_3$ micro-ellipsoids were fabricated, and its optimized operating temperature, response/recovery time, long-term stability and selectivity to $H_2S$ gas were investigated.

## 2. Materials and methods

### 2.1 Synthesis process

All the reagents (with analytical-grade purity) were purchased from Sinopharm Chemical Reagent Co., Ltd, China, and used as-received without any further purification. The α-$Fe_2O_3$ micro-ellipsoids were synthesized based on a hydrothermal reaction. In a typical synthesis process, $FeCl_3 \cdot 9H_2O$ of 8.109 g was dissolved in the distilled water of 100 ml under a continuous stirring at room temperature to form a 0.3 mol /L $FeCl_3 \cdot 9H_2O$ (light red) homogeneous solution. Subsequently, 50 ml of NaOH (0.6 mol /L) was dripped into the above solution in 10 minutes, and continually stirred at the room temperature for 30 minutes to get a reddish brown $Fe(OH)_3$ sol. The obtained $Fe(OH)_3$ sol was transferred into two Teflon-lined stainless steel autoclaves of 150 ml and kept at 170 $^oC$ for 8 hours. Subsequently, the autoclave was cooled down to room temperature naturally. The resultant rufous precipitate was collected and washed using centrifugation with distilled water and absolute ethanol for three times, respectively. Then it was dried at 80 $^oC$ in air for two hours. After cooling down room temperature, the rufous α-$Fe_2O_3$ micro-ellipsoids were obtained. They were then annealed at 400 $^oC$ for one hour in air before used as the sensing material.

### 2.2 Characterization methods

Crystal structures and phase composition of the α-$Fe_2O_3$ micro-ellipsoids were characterized using X-ray diffraction (XRD, Rigaku D/max-2500) with Cu Kα radiation at a wavelength of 1.5406 Å and operating voltage/current of 40 kV/30 mA. The morphologies of the micro-ellipsoids were observed using a scanning electron microscope (SEM, Inspect F50, USA) with an operation voltage of 5 kV. Transmission electron microscope (TEM, JEM-2200FS, Japan) was used to characterize crystallographic features of the sample. Surface porosity was characterized using a method of nitrogen

adsorption isotherms, measured using a BELSORP-miniII (Japan) analyzer at 77.4 K. Before measurements, the samples were degassed at 200 °C in a vacuum (with a based vacuum of $10^{-6}$ Pa) for more than 6 hours. Brunauer-Emmett-Teller (BET) method was utilized to calculate the specific surface areas, and the total pore volumes ($V_{tot}$) were estimated from the adsorbed amounts of nitrogen at a relative pressure P/P0 of 0.99. Chemical states of elements for the $Fe_2O_3$ samples were analyzed using X-ray photoelectron spectroscopy (XPS, KratosAxis-Ultra DLD, Japan) with a monochromatic Al Kα radiation (1486.6 eV). Both survey scan and detailed scan of different elements have been recorded using the XPS. The Fourier transform infrared spectrum (FT-IR) was measured using Nicolet 380.

**2.3 Gas sensor fabrication and measurements**

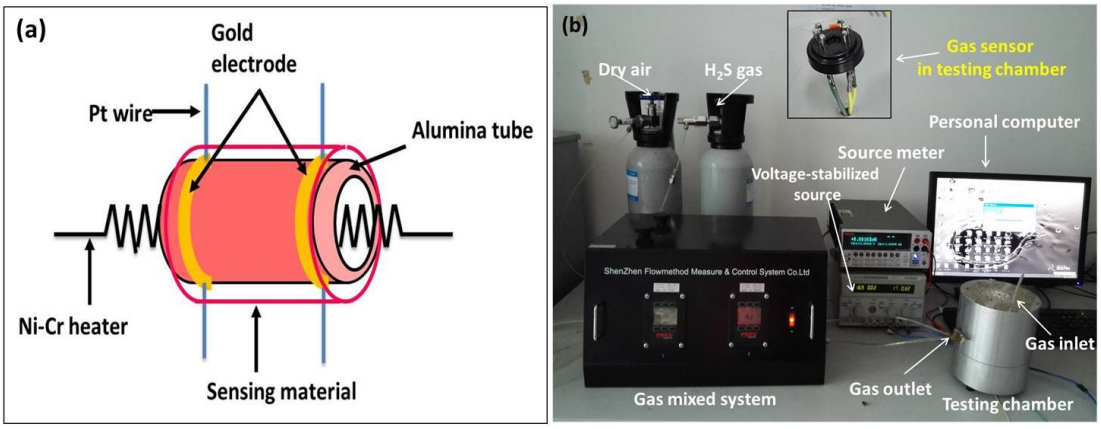


**Figure 1** (a) Schematic gas sensor based on α-$Fe_2O_3$ micro-ellipsoids. (b) The measurement setup for the gas sensor.

The schematic illustration of the gas sensor is shown in Fig. 1a. In the alumina tube, there was a Ni-Cr heater to control the working temperature of the sensor through varying the heating voltage. There were a pair of gold electrodes on the surface of alumina tube. Platinum wires were used to connect the gold electrodes with the testing electric circuit. The fabrication process of sensing materials layer of α-$Fe_2O_3$ micro-ellipsoids could be described as follows. Firstly, as-prepared powders of the α-$Fe_2O_3$ micro-ellipsoids were mixed with alcohol to form homogeneous slurry. Then the slurry was

pasted onto the alumina tube. Finally, the alumina tube was calcined at 300 $^{o}$C for 2 hours to improve the stability of the sensors.

Fig. 1b shows the measurement setup for the gas sensor. The gas sensor was placed inside a 400 ml testing chamber. The concentration of target gas and flow rate were controlled using a gas mixing system, by controlling the ratio between the target gas and dry air using two mass flow controllers. During testing, an appropriate working voltage (Vs=5 V) was applied. Changes of resistance of the gas sensor were measured using a source meter (Keithley 2400) and the data were collected using a Lab-view software. The respond (R) of the sensor is defined as follows: R=Ra/Rg, where the Rg and Ra are the resistance of the sensor in $H_2S$ gas and air, respectively [30].

## 3. Results and Discussions

### 3.1 Structural and morphological characteristics

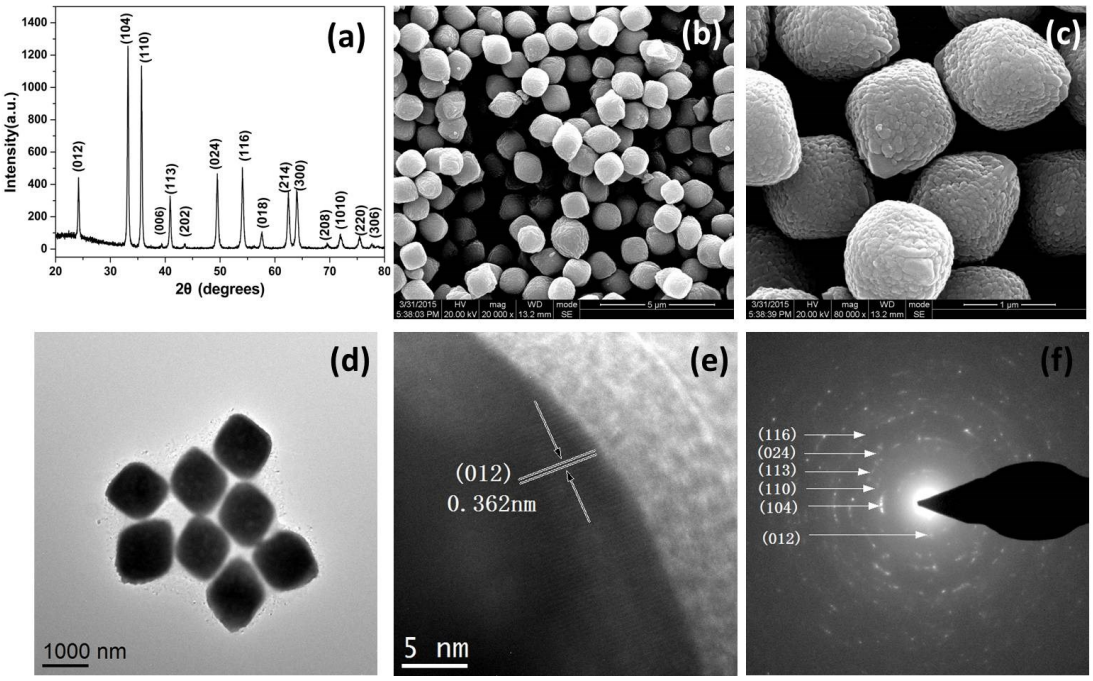


**Figure 2** (a) XRD pattern; (b, c) SEM images; (d) wide-field TEM image; (e) HRTEM image; (f) selected area electron diffraction pattern (SAED) of α-$Fe_2O_3$ ellipsoids.

Fig. 2a shows the XRD pattern of the α-$Fe_2O_3$ micro-ellipsoids. All the diffraction peaks were linked

with the standard hexagonal structure of hematite (α-$Fe_2O_3$) reflection (JCPDS NO.33-0664) with the calculated lattice parameters of a=b=5.0297Å, c=13.7340Å and α=β=90°, γ=120°. No characteristic peaks from the other iron oxide were identified, indicating that the samples were pure α-$Fe_2O_3$. Furthermore, the crystallite grain size of the α-$Fe_2O_3$ was estimated to be 152.8 nm according to the Scherrer formula:

$$L = K\lambda /(\beta \cos\theta) \quad (1)$$

Where $\lambda$ is the wavelength of the X-ray radiation (0.15406 nm for Cu Kα); $K$ is a constant taken as 0.89; $\beta$ is the line width at half maximum height and $\theta$ is the diffracting angle.

Fig. 2b and Fig. 2c present typical SEM images of the α-$Fe_2O_3$ micro-ellipsoids. It can be seen that the samples are composed of uniform micro-particles with a long axis diameter of 1.7 μm and a short axis diameter of 1.2 μm. The α-$Fe_2O_3$ micro-ellipsoids were composed of nanoparticles with diameters of 50-180 nm. The measured BET surface areas and pore volumes of α-$Fe_2O_3$ micro-ellipsoids were 2.28 $m^2 \cdot g^{-1}$ and 0.0007 $cm^2 \cdot g^{-1}$, respectively. These low values of surface areas and pore volumes indicated that the α-$Fe_2O_3$ micro-ellipsoids were compact nonporous particles. The structure of α-$Fe_2O_3$ micro-ellipsoids was different from the other types of reported $Fe_2O_3$ ellipsoids. For example, Abaker et al [31] prepared nano-ellipsoids using the hydrothermal process with central diameters of 40 nm and lengths of 100 nm; Freyria et al [32] reported rain-like $Fe_2O_3$, but it was nano-particle, rather than micro-particle.

Fig. 2d shows a low magnification TEM image of the as-prepared α-$Fe_2O_3$ micro-ellipsoids. Clearly, the α-$Fe_2O_3$ powder showed a uniform ellipsoid morphology. A series of clear and continuous lattice fringes could be seen from the high-resolution TEM (HRTEM) image (Fig. 2e) of the α-$Fe_2O_3$ micro-ellipsoids. The typical lattice fringe spacing was determined to be 0.362 nm, which is

corresponding to the d-spacing of the (012) planes of hexagonal α-$Fe_2O_3$. The well crystallized nature of the α-$Fe_2O_3$ micro-ellipsoids could be confirmed based on the selected area electron diffraction (SAED) patterns as shown in Fig. 2f. The diffraction rings in the pattern could be indexed to (012), (104), (110), (113), (024), (116) lattice planes of the hexagonal α-$Fe_2O_3$, which agree well with the results from the XRD analysis as shown in Fig. 2a.

Based on these results, the formation mechanism of the α-$Fe_2O_3$ could be described as follows. When NaOH solution was introduced into the $FeCl_3$ solution, amorphous $Fe(OH)_3$ sol was formed according to the following reaction (2):

$$FeCl_3 \cdot 6H_2O + 3NaOH \rightarrow Fe(OH)_3 + 3NaCl + 6H_2O \quad (2)$$

$$Fe(OH)_3 \rightarrow FeOOH + H_2O \quad (3)$$

$$2FeOOH \rightarrow \alpha\text{-}Fe_2O_3 + H_2O \quad (4)$$

In the hydrothermal process, the amorphous $Fe(OH)_3$ was dissolved and FeOOH was formed as according to the chemical reaction equations (3). Under the high pressure and high temperature conditions, the FeOOH nanoparticles were combined together by self-assembly and transformed into hexagonal phase α-$Fe_2O_3$ micro-ellipsoids.

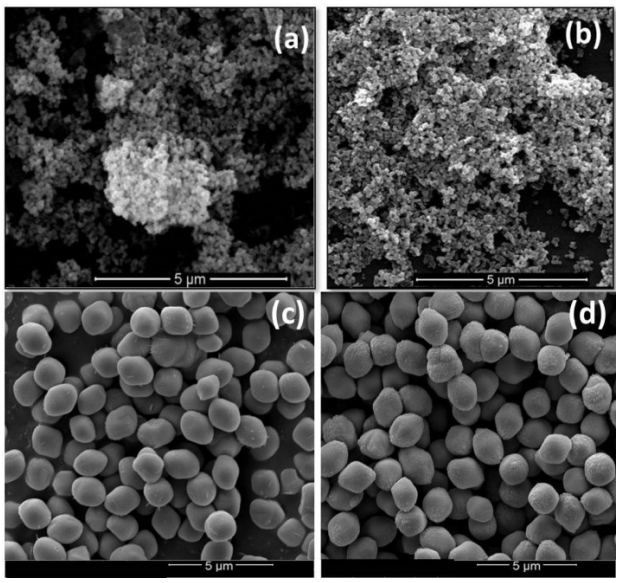

**Figure 3** SEM images of α-$Fe_2O_3$ by the hydrothermal reaction (a) at 170 $^oC$ for 2 hours; (b) at 140 $^oC$ for 8 hours; (c) at 170 $^oC$ for 4 hours; (d) at 190 $^oC$ for 8 hours.

The effects of the temperature and time of hydrothermal reaction on the morphology and size of the products were investigated. When the time of the hydrothermal reaction in the Teflon-lined stainless steel autoclave at 170 $^oC$ was fixed at 2 hours, the product was spherical nanoparticles with an average diameter of 128 nm as shown in Fig. 3a. At a lower hydrothermal temperature of 140 $^oC$ for 8 hours, the synthesized product was spherical nanoparticles with an average diameter of 115 nm as shown in Fig. 3b. However, when the reaction time was increased to 4 hours at 170 $^oC$ or the reaction temperature was increased to 190 $^oC$ for 8 hours, the products were uniform micro-ellipsoids as shown in Fig. 3c and Fig. 3d, which were same as the sample prepared at 170 $^oC$ for 8 hours

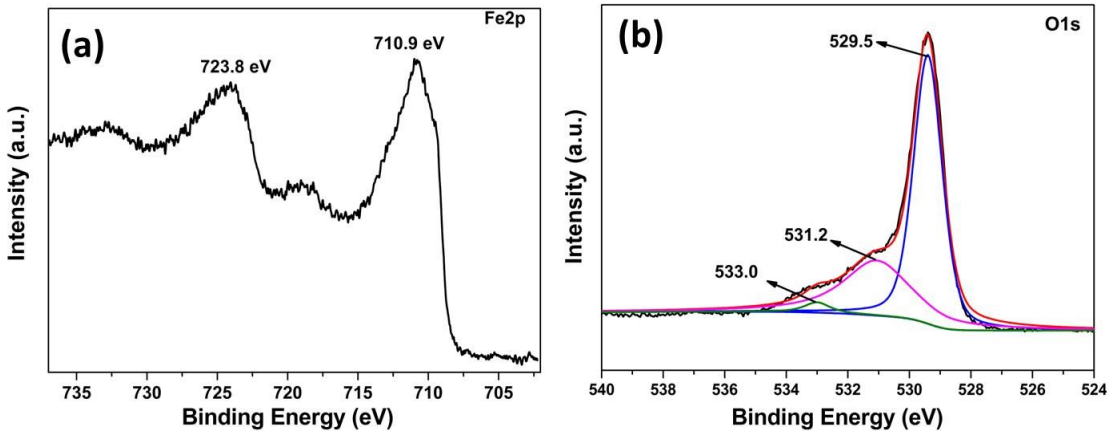


**Figure 4** (a) Fe 2p and (b) O 1s of α-$Fe_2O_3$ micro-ellipsoids obtained from the XPS analysis.

The XPS analysis results of the α-$Fe_2O_3$ micro-ellipsoids are shown in Fig. 4. The dominant binding energy peaks at 723.8 and 710.9 eV proved that the chemical state in the prepared α-$Fe_2O_3$ micro-ellipsoids is $Fe^{3+}$ as shown in Fig. 4a [30,33]. Three obvious peaks could be identified from the O 1s spectrum, i.e., 529.5, 531.2 and 533.0 eV, as shown in Fig. 4b. The peak located at 529.5 eV is corresponding to lattice oxygen atoms in the α-$Fe_2O_3$. The peaks located at 531.2 and 533.0 eV could be attributed to oxygen species and the water molecule which are absorbed on the surface, respectively

[33].

### 3.2 Gas sensing properties

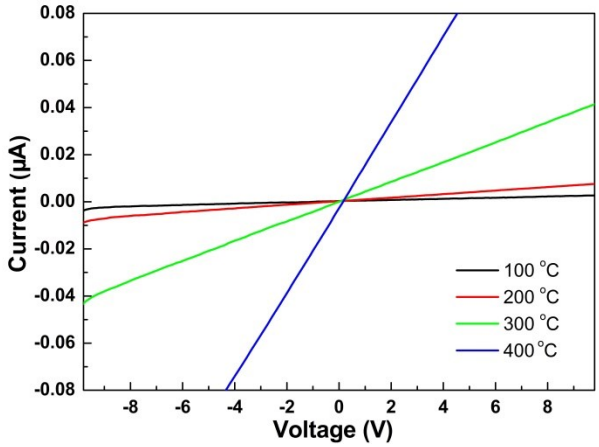


**Figure 5** I-V curves of α-$Fe_2O_3$ micro-ellipsoids based sensor at different working temperatures.

Fig. 5 shows typical current-voltage (I-V) curves between the two neighboring platinum electrodes bridged by the α-$Fe_2O_3$ micro-ellipsoid layer at different working temperatures from 100 °C to 400 °C. It can be seen that all the currents were increased linearly with the applied bias voltage (from -10 V to 10 V). Such a perfectly linear behavior revealed that the good ohmic contacts were formed between the α-$Fe_2O_3$ micro-ellipsoid layer and electrodes. Moreover, with the increase of the working temperature, the conductance (S=I/V) of the α-$Fe_2O_3$ micro-ellipsoid layer was increased, which is in agreement with the conduction characteristics of a typical semiconductor.

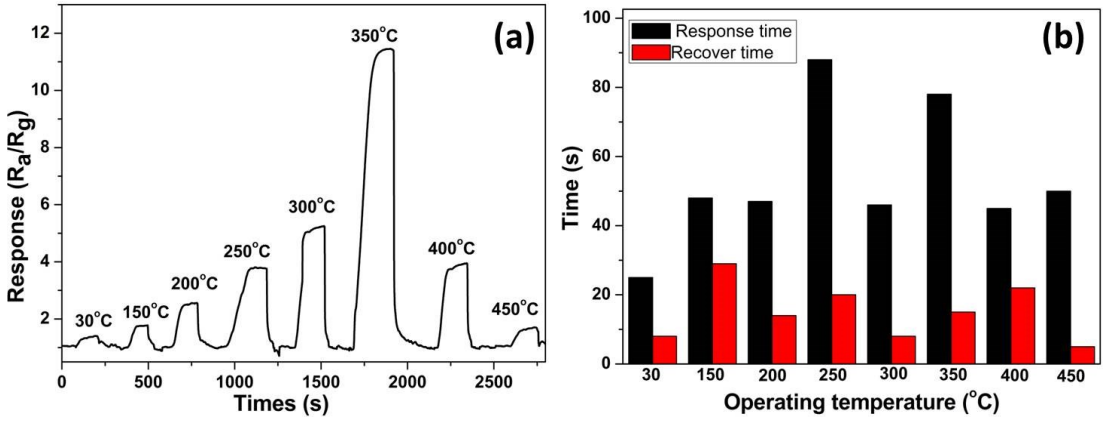


**Figure 6** (a) Dynamic response/recovery curves and (b) Response time and recovery time of the α-$Fe_2O_3$ micro-ellipsoid gas sensor to $H_2S$ gas of 100 ppm at different working temperatures.

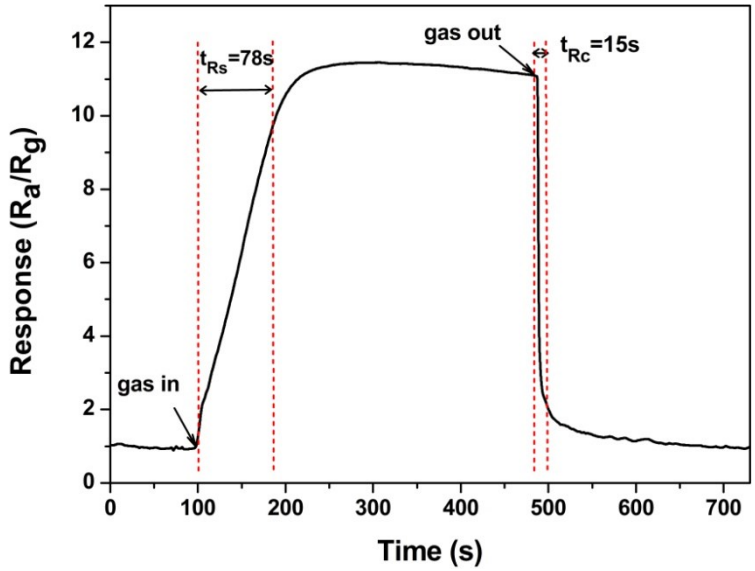


**Figure 7** Real-time gas sensing transients of the sensor based on α-$Fe_2O_3$ micro-ellipsoids to 100 ppm $H_2S$ gas at 350 $^oC$.

It is well known that the operating temperature has a significant effect on gas-sensing performance of gas sensors. Therefore, in order to find the optimum operating temperature of the $H_2S$ gas sensor, the responses of the sensor based on α-$Fe_2O_3$ micro-ellipsoids to the $H_2S$ gas were measured at different working temperatures from 30 $^oC$ to 450 $^oC$. As shown in Fig. 6a, the sensing responses of the sensors to the $H_2S$ gas of 100 ppm increased with the operating temperature increased from 30 $^oC$ to 350 $^oC$. The sensing response values had a maximum at 350 $^oC$ with a response of 11.7. Then, the response value was decreased with a further increase of temperature from 350 $^oC$ to 450 $^oC$. Therefore, the optimum operating temperature of the α-$Fe_2O_3$ micro-ellipsoids based $H_2S$ sensor was 350 $^oC$.

The increase in gas response at the operating temperatures from 30 $^oC$ to 350 $^oC$ could be attributed to the fact that the obtained thermal energy was in favor of overcoming the activation energy barrier for the surface chemical reactions between $H_2S$ molecules and absorbed oxygen species, causing the significant increase of response of gas sensor to $H_2S$ [34-36]. However, when the operating temperature

was above 350 $^{o}$C, the $H_2S$ gas was consumed within a very shallow surface of the sensing layer, therefore, the utilization rate of the sensing layer was decreased, thus the diffusion depth of the $H_2S$ gas was decreased [34-36]. Accordingly, the resistance of sensor was decreased.

The response and recovery time were defined as the time to achieve 90% of the total resistance change in the case of injection and extraction of $H_2S$, respectively. From Fig. 6b, the gas sensor based on the α-$Fe_2O_3$ micro-ellipsoids obviously shows rapid response (less than 90s) and recovery time (less than 30s) at different operating temperatures. Considering all the response results of the sensors operated at different temperatures, the temperature of 350 $^{o}$C was chosen as the optimum temperature to investigate its sensing properties. Fig. 7 displays the real-time transients for the gas sensing of the sensor based on α-$Fe_2O_3$ micro-ellipsoids when exposed to 100 ppm $H_2S$ gas at 350 $^{o}$C. The response time and recovery time were determined to be 78 s and 15 s, respectively. The almost square shape of the response curve indicated that the sensor had a rapid response to the $H_2S$ gas. When the sensor was exposed to air again, the response of the senor could be returned near to the baseline level.

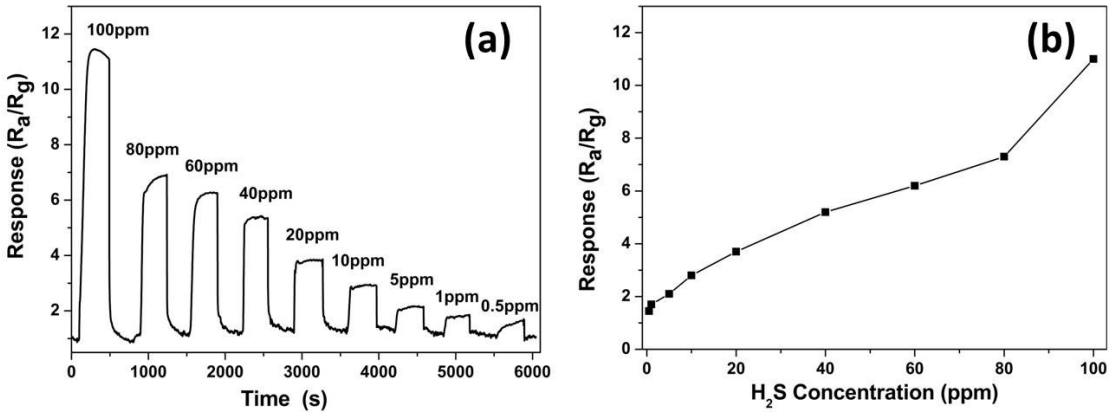


**Figure 8** (a) Dynamic response-recovery curve and (b) response of the α-$Fe_2O_3$ micro-ellipsoids based sensor to $H_2S$ gas at the working temperature of 350 $^{o}$C.

The response and recovery behaviors of the sensor to different concentrations of the $H_2S$ gas were further investigated at the operating temperature of 350 $^{o}$C, and the results are shown in Fig. 8. It can

be seen that the response was increased with increasing $H_2S$ concentration. At a low $H_2S$ concentration of 0.5 ppm, the α-$Fe_2O_3$ micro-ellipsoids based sensor still showed an excellent response of 1.45 and a fast response time of 80 s and a recovery time of 7 s. The electrical resistance values of the sensor decreased quickly as soon as the $H_2S$ gases with different concentrations were injected into chamber but then recovered quickly to its initial values once the test chamber was refreshed with air, indicating good repeatability and reversibility of the sensor. The SEM images proved that the surfaces of α-$Fe_2O_3$ micro-ellipsoids were composed of nanoparticles with diameters of 50-180 nm, which were in favor of the diffusion and adsorption of $H_2S$ gas. Therefore, the $H_2S$ gas sensor has good response and short response/recovery time.

Table 1 Comparison of $H_2S$ sensing properties of different metal oxide based gas sensor.

| Metal oxide | Working temperature ($^oC$) | Detection Limit (ppm) | Response/recovery time | Reference |
|---|---|---|---|---|
| $Co_3O_4$ nanoparticles | 250 | 5 | 1 min/5 min | [37] |
| CuO nanoparticles | 80 | 10 | 20 s/60 s | [38] |
| $SnO_2$ nanotubes | 300 | 100 | 60 s/90 s | [39] |
| Porous α-$Fe_2O_3$ | 330 | 5 | 1 s/10 s | [40] |
| $Fe_2O_3$ thin films | 250 | 1 | 64 s /390 s | [41] |
| α-$Fe_2O_3$ nanoparticles | 160 | 50 | 68 s/35 s | [42] |
| $Fe_2O_3$ thin films | 250 | 1 | 1.65 min/27 min | [43] |
| α-$Fe_2O_3$ micro-ellipsoids | 350 | 0.5 | 80 s/7 s | Our work |

The sensing properties of the α-$Fe_2O_3$ micro-ellipsoids were compared to other metal oxide based $H_2S$ sensors reported in literature, and the results are listed in Table 1. It can be seen that the gas sensor based on the α-$Fe_2O_3$ micro-ellipsoids exhibited a better sensing performance with a lower detection concentration and more immediate response/recovery times of 80s/7 s, respectively.

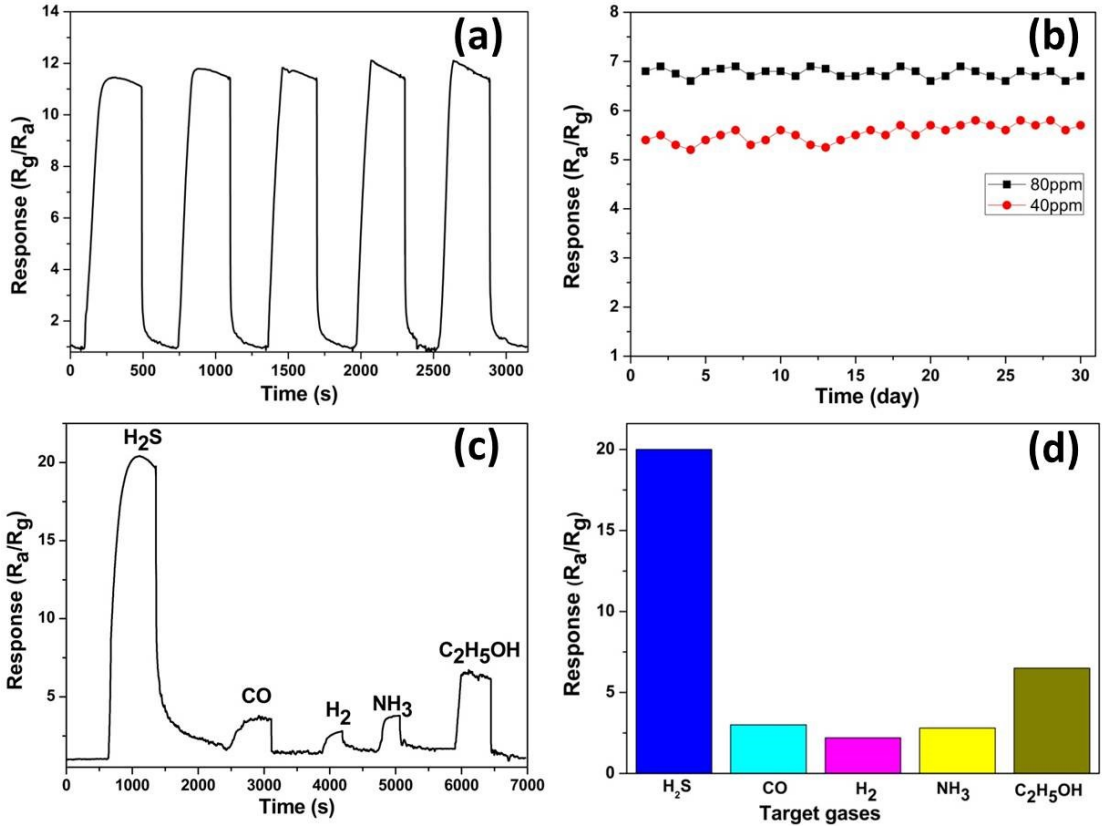


**Figure 9** (a) Reproducibility of the sensor based on α-$Fe_2O_3$ micro-ellipsoids by repetitively exposing it to 100 ppm $H_2S$ gas at 350 $^oC$; (b) The response of $H_2S$ gas sensor based on α-$Fe_2O_3$ micro-ellipsoids to 40 ppm and 80 ppm for 30 days at 350 $^oC$; (c) Dynamic response-recovery curve and (d) Response histogram of α-$Fe_2O_3$ micro-ellipsoids based gas sensor towards different gases at the same concentration of 400 ppm at 350 $^oC$.

Fig. 9a shows the reproducibility of the α-$Fe_2O_3$ micro-ellipsoids based sensor exposed to the $H_2S$ gas at a concentration of 100 ppm for 5 cycles. There was a stable response curve with a maximum response of 11.7 to 100 ppm $H_2S$. During the repeated processes of $H_2S$ gas injection and release, the response-recovery curves of the sensor were almost identical, indicating the good reproducibility of the α-$Fe_2O_3$ micro-ellipsoids based gas sensor. The long-term stability of the $H_2S$ gas sensor based on the α-$Fe_2O_3$ micro-ellipsoids was also investigated. The response to the $H_2S$ gas of 40 ppm and 80 ppm for 30 days at 350 $^oC$ are shown in Fig. 9b. It could be seen that there were no significant changes in

current responses during the continuous measurement for 30 days, meaning that the sensor had an excellent long-term stability for $H_2S$ detection.

The sensing responses of the α-$Fe_2O_3$ micro-ellipsoids based sensor to several reducing gases ($H_2S$, $C_2H_5OH$, CO, $H_2$, $NH_3$) were measured using a fixed gas concentration of 400 ppm at 350 $^oC$, and the results are shown in Fig. 9c and Fig. 9d. It can be seen that the gas sensor showed a remarkably better response to $H_2S$ gas than the other gases at the same testing conditions. The gas response to the $H_2S$ was 3.1 times as high as that to $C_2H_5OH$, 7 times as those to CO and $NH_3$, and 9.1 times as that to $H_2$, respectively, suggesting that the sensor had an excellent selectivity toward $H_2S$ gas.

**3.3 Gas sensing mechanism**

The α-$Fe_2O_3$ is an n-type metal oxide semiconductor and its sensing property is governed by the change of the resistance resulted from the chemical interactions between the target gas and the oxygen species absorbed on the surface of the sensor [44, 45]. When the α-$Fe_2O_3$ was exposure to the air, the oxygen molecules were absorbed on the surface of α-$Fe_2O_3$, and then formed negatively charged chemisorbed oxygen species ($O_2^-$, $O^-$, $O^{2-}$) by capturing electrons from conduction bands and trapped them at the surface. The types of absorbed oxygen species were dependent on the working temperature. When the temperature was lower than 100 $^oC$, $O_2^-$ was commonly chemisorbed. However, when the temperature was between 100 $^oC$ and 300 $^oC$, $O^-$ became commonly chemisorbed and the $O_2^-$ disappeared rapidly. Once the temperature was higher than 300 $^oC$, the oxygen species were mainly existed in the form of $O^{2-}$ [46]. The absorption processes on the surface could be explained as follows:

$$O_{2(g)} \rightarrow O_{2(ad)} \quad (5)$$

$$O_{2(ad)} + e^- \rightarrow O_{2(ad)}^- \quad (T < 100\ ℃) \quad (6)$$

$$O_{2(ad)}^- + e^- \rightarrow 2O_{(ad)}^- \quad (100\ ℃ < T < 300\ ℃) \quad (7)$$

$$O^-_{(ad)} + e^- \rightarrow O^{2-}_{(ad)} \qquad (T > 300\,℃) \qquad (8)$$

The dominant species on the surface of α-$Fe_2O_3$ at 350 °C was $O^{2-}$ [44]. Therefore, the conduction mechanism of the sensor was mainly governed by the following reaction equation [47, 48]:

$$H_2S_{(g)} + 3O^{2-}_{(ad)} \leftrightarrow H_2O_{(g)} + SO_{2(g)} + 6e^- \qquad (6)$$

Upon exposed to $H_2S$ gas, sulfur dioxide ($SO_2$) was formed on the sensor surface and the free charge carriers were injected into the conduction band, thus resulting in the decrease in resistance of the sensor.

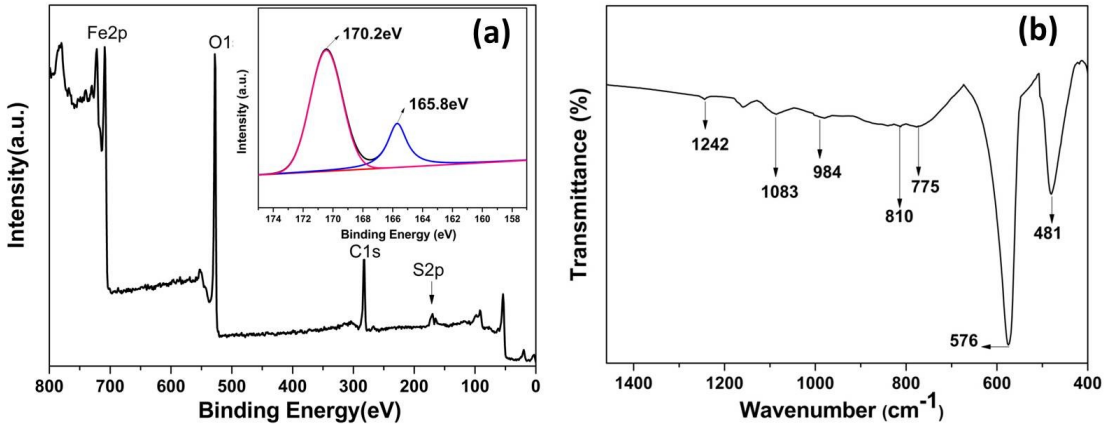


Fig.10 (a) Wide range XPS spectrum (inset is high resolution spectrum of S 2p) and (b) FT-IR spectrum of α-$Fe_2O_3$ micro-ellipsoids after exposure to $H_2S$ gas.

To confirm the formation of $SO_2$, XPS analysis after exposure to the sensor to $H_2S$ gas were performed (as shown in Fig. 10a). It can be seen that there were peaks of S element in the XPS spectrum. The fitted curve of high resolution spectrum of S 2p (see the inset of Fig. 10a) shows two peaks at 165.8 eV and 170.2 eV, which were assigned to $SO_2$ and the residual $H_2S$ absorbed on the material surface, respectively [49]. Therefore, formation of the $SO_2$ can be confirmed during surface reaction. The FT-IR spectrum after adsorption $H_2S$ gas is shown in Fig. 10b. The peaks at 481 $cm^{-1}$ and 576 $cm^{-1}$ could be attributed to the Fe–O vibration of α-$Fe_2O_3$. The region from 700 $cm^{-1}$ to1350 $cm^{-1}$ was related to sulfate groups. The peak at 1242 $cm^{-1}$ was attributed to the asymmetrically $SO_2$

stretching vibration. The peaks at 1083 cm−1 and 984 $cm^{-1}$ were attributed to the stretching vibration of S-O bond. The peaks at 775 $cm^{-1}$ and 810 $cm^{-1}$ could be corresponded to S–O stretching vibration. Thus, the IR results also proved the formation of sulfate oxides on the surface of α-$Fe_2O_3$ due to reaction of $H_2S$ with oxygen species on the surface.

## 4. Conclusions

In summary, the uniform α-$Fe_2O_3$ micro-ellipsoids structure could be prepared directly from solution without any surfactant using a facile hydrothermal process. The α-$Fe_2O_3$ micro-ellipsoids were compact nonporous particles with a long axis diameter of 1.7 μm and a short axis diameter of 1.2 μm. At the optimal operating temperature of 350 $^oC$, the α-$Fe_2O_3$ micro-ellipsoids based $H_2S$ gas sensor have good sensing performance including low detection concentration, rapid response/recovery time, good long-term stability and excellent response. Therefore, the α-$Fe_2O_3$ micro-ellipsoids prepared in this study can be efficiently used for high-performance $H_2S$ gas sensor.

## Acknowledgments

This work was supported by the Joint Fund of the National Natural Science Foundation of China and the China Academy of Engineering Physics (U1330108), the UOA and CAPEX Funding from Northumbria University at Newcastle upon Tyne, and Royal Academy of Engineering UK-Research Exchange with China and India.

## References

[1] L. Yue, K.H Wang, J.B. Guo, , J.L. Yang, X. Luo, J. Lian, L. Wang, Enhanced electrochemical oxidation of dye wastewater with $Fe_2O_3$ supported catalyst, J. Ind. Eng. Chem. 20 (2014) 725–731.

[2] H. Katsuki, S. Komarneni, Role of α-$Fe_2O_3$ morphology on the color of red pigment for porcelain, J. AM. Ceram. Soc. 86 (2003) 183–185.

[3] J.T. Wu, S.Y. Mao, Z.G. Ye, Z.X. Xie, L.S. Zheng, Room-temperature weak ferromagnetism induced by point defects in alpha-$Fe_2O_3$, ACS Appl. Mater. Inter. 2 (2010) 1561–1564.

[4] L.L. Li, Y. Chu, Y. Liu, L.H. Dong, Template-free synthesis and photocatalytic properties of novel $Fe_2O_3$ hollow spheres, J. Phys. Chem. C 111 (2007) 2123–2127.

[5] M.H. Chen, J.L. Liu, D.L. Chao et al, Porous alpha-$Fe_2O_3$ nanorods supported on carbon nanotubes-graphene foam as superior anode for lithium ion batteries, Nano Energy 9 (2014) 364–372.

[6] X.M. Lou, J.L. Huang, T.P. Li, H.X. Hu, B.N. Hu, Y.X. Zhang, Hydrothermal synthesis of $Fe_3O_4$ and α-$Fe_2O_3$ nanocrystals as anode electrode materials for rechargeable Li-ion batteries, J. Mater. Sci: Mater Electron 25 (2014) 1193–1196.

[7] X.H. Liu, J. Zhang, X.Z. Guo, S.H. Wu, S.R. Wang, Porous α-$Fe_2O_3$ decorated by Au nanoparticles and their enhanced sensor performance, Nanotechnology 21 (2010) 095501.

[8] J.S. Han, D.E. Davey, D.E. Mulcahy, A.B. Yu, Effect of the pH value of the precipitation solution on the CO sensitivity of α-$Fe_2O_3$, Sens. Actuators B: Chem 61 (1999) 83–91.

[9] P. Sun, W.N. Wang, Y.P. Liu, Y.F. Sun, J. Ma, G.Y. Lu, Hydrothermal synthesis of 3D urchin-like-$Fe_2O_3$ nanostructure for gas sensor, Sens. Actuators B: Chem 173 (2012) 52–57.

[10] G. Neri, A. Bonavita, S. Galvagno, P. Siciliano, S. Capone, CO and $NO_2$ sensing properties of doped-$Fe_2O_3$ thin films prepared by LPD, Sens. Actuators B: Chem 82 (2002) 40–47.

[11] G.K. Fan, Y. Wang, M. Hu, Z.Y Luo, Kaihuan Zhang, G. Li, Template Free Synthesis of Hollow Ball-Like Nano-$Fe_2O_3$ and Its Application to the Detection of Dimethyl Methylphosphonate at Room

Temperature, Sensors 12 (2012) 4594–4604.

[12] X. Zhou, C. Wang, W. Feng, P. Sun, , X.W. Li, G.Y. Lu, Hollow α-$Fe_2O_3$ quasi-cubic structures: Hydrothermal synthesis and gas sensing properties, Mater. Lett. 120 (2014) 5–8.

[13] D. Patil, V. Patil, P. Patil, Highly sensitive and selective LPG sensor based on α-$Fe_2O_3$ nanorods, Sens. Actuators B: Chem 152 (2011) 299–306.

[14] Y. Wang, J.L. Cao, S.R. Wang, X.Z. Guo, J. Zhang, H.J. Xia, S.M. Zhang, S.H. Wu, Facile Synthesis of Porous r-$Fe_2O_3$ Nanorods and Their Application in Ethanol Sensors, J. Phys. Chem. C 112 (2008) 17804–17808.

[15] D.K. Bandgar, S.T. Navale, A.T. Mane, S.K. Gupta, D.K. Aswal, V.B. Patil, Ammonia sensing properties of polyaniline/a-$Fe_2O_3$ hybrid nanocomposites, Synthetic Met. 204 (2015) 1–9.

[16] D.K. Bandgar, S.T. Navale, G.D. Khuspe, S.A. Pawar, R.N. Mulik, V.B. Patil, Novel route for fabrication of nanostructured α-$Fe_2O_3$ gas sensor, Mat. Sci. Semiccon. Proc. 17(2014)67–73.

[17] S.T. Navale, D.K. Bandgar, S.R. Nalage, G.D. Khuspe, M.A. Chougule, Y.D. Kolekar, S. Shashwati, V.B. Patil, Synthesis of $Fe_2O_3$ nanoparticles for nitrogen dioxide gas sensing applications, Ceram. Int. 39 (2013) 6453–6460.

[18]V. V. Jadhav, S. A. Patil D. V. Shinde, S. D. Waghmare, M. K. Zate , R. S. Mane, Sung-Hwan Han Hematite nanostructures: Morphology-mediated liquefied petroleum gas sensors, Sens. Actuators B: Chem 188 (2013) 669–674.

[19] L. Liao, Z. Zheng, B. Yan, J.X. Zhang, H. Gong, J.C. Li, C. Liu, Z.X. Shen, T. Yu, Morphology Controllable Synthesis of α-$Fe_2O_3$ 1D Nanostructures: Growth Mechanism and Nanodevice Based on Single Nanowire, J. Phys. Chem. C 112 (2008) 10784–10788.

[20] T.P. Almeida, M.W. Fay, Y.Q. Zhu, P.D. Brown, In situ TEM investigation of β-FeOOH and

α-$Fe_2O_3$ nanorods, Physica. E 44 (2012) 1058–1061.

[21] C.Z. Wu, P. Yin, X. Zhu, Y. Xie, Synthesis of hematite (α-$Fe_2O_3$) nanorods: diameter-size and shape effects on their applications in magnetism, lithium ion battery, and gas sensor, J. Phys. Chem. B 110 (2006) 17806-17812.

[22] Z.P. Cheng, X.Z. Chu, J.Z. Yin, H. Zhong, J.M. Xu, Surfactantless synthesis of $Fe_3O_4$ magnetic nanobelts by a simple hydrothermal process, Mater. Lett. 75 (2012) 172–174.

[23] W. Zheng, Z.Y. Li, H.N. Zhang, W. Wang, Y. Wang, C. Wang, Electrospinning route for α-$Fe_2O_3$ ceramic nanofibers and their gas sensing properties, Mater. Res. Bull 6 (2009) 1432–1436.

[24] L. Xia, J.G. Ju, W. Xu, C.K. Ding, B.W. Cheng, Preparation and characterization of hollow $Fe_2O_3$ ultra-fine fibers by centrifugal spinning, Mat. Des. 96 (2016) 439–445.

[25] S.W. Cao, Y.J. Zhu, Hierarchically nanostructured α-$Fe_2O_3$ hollow spheres: preparation, growth mechanism, photocatalytic property, and application in water treatment, J. Phys. Chem. C 112 (2008) 6253–6257.

[26] Z. Sun, H. Yuan, Z. Liu, B. Han, X. Zhang, A highly efficient chemical sensor material for $H_2S$: α-$Fe_2O_3$ nanotubes fabricated using carbon nanotube templates, Adv. Mater. 17 (2005) 2993–2997.

[27] L. Liu., H.Z. Kou, W.L. Mo, H.J. Liu, Y.Q. Wang, Surfactant-assisted synthesis of alpha-$Fe_2O_3$ nanotubes and nanorods with shape-dependent magnetic properties, J. Phys. Chem. B 110 (2006) 15218–15223.

[28] S.K. Mohapatra, S.E. John, S. Banerjee, Water photooxidation by smooth and ultrathin α-$Fe_2O_3$ nanotube arrays, Chem. Mater. 21 (2009) 3048–3055.

[29] J.W. Deng, J.M. Ma, L. Mei, Y.J. Tang, Y.J Chen, T. Lv, Z. Xu, T.H. Wang, Porous α-$Fe_2O_3$ nanosphere-based $H_2S$ sensor with fast response, high selectivity and enhanced sensitivity, J. Mater.

Chem. A 1 (2013) 12400–12403.

[30] Y.W. Huang, W.M. Chen, S.C. Zhang, Z. Kuang, D.Y Ao, N. R. Alkurd, W.L. Zhou, W. Liu, W.Z. Shen, Z.J Li, A high performance hydrogen sulfide gas sensor based on porous α-$Fe_2O_3$ operates at room-temperature, Appl. Surf. Sci. 351 (2015) 1025–1033.

[31] M. Abaker, A. Umar, S. Baskoutas, G.N. Dar, S.A. Zaidi, S. A. Al-Sayari, A. Al-Hajry, S.H. Kim and S.W. Hwang, A highly sensitive ammonia chemical sensor based on α-$Fe_2O_3$ nanoellipsoids, J. Phys. D: Appl. Phys. 44 (2011) 425401.

[32] F.S. Freyria, G. Barrera, P. Tiberto, E. Belluso, D. Levy, G. Saracco, P. Allia, E. Garrone, B. Bonelli, Eu-doped α-$Fe_2O_3$ nanoparticles withmodified magneticproperties, J. Solid State Chem. 201 (2013) 302–311.

[33] Y. Wang, S.R. Wang, Y.Q. Zhao, B.L. Zhu, F.H. Kong, D. Wang, S.H. Wu, , W.P. Huang, S.M. Zhang, $H_2S$ sensing characteristics of Pt-doped alpha-$Fe_2O_3$ thick film sensors, Sens. Actuators B: Chem 125 (2007) 79–84.

[34] N. Yamazoe, J. Fuchigami, M. Kishikawa, T. Seiyama, Interactions of tin oxide surface with $O_2$, $H_2O$ and $H_2$, Surf. Sci. 86 (1979) 335–344.

[35] J. Chen, K. Wang, L. Hartman, W. Zhou, $H_2S$ detection by vertically aligned CuO nanowire array sensors, J. Phys. Chem. C 112 (2008) 16017–16021.

[36] P. Sun, X. Zhou, C. Wang, K. Shimanoe, G.Y. Lu, N. Yamazoe, Hollow $SnO_2$/α-$Fe_2O_3$ spheres with a double-shell structure for gas sensors, J. Mater. Chem. A 2 (2014) 1302–1308.

[37] S. Moon, N. M. Vuong, D. Lee, D. Kim, H. Lee, D. Kim, H. Soon-Ku, Y. Soon-Gil, $Co_3O_4$ – SWCNT composites for H2S gas sensor application, Sens. Actuators B: Chem 222 (2016) 166–172.

[38] A. I. Ayesh, F.S. Ayah, Abu-Hani, S. T. Mahmoud, Y. Haik; Selective $H_2S$ sensor based on CuO

nanoparticles embedded in organic membranes, Sens. Actuators B: Chem 231 (2016) 593–600.

[39] N.Y. Zhao, Z. Chen, W. Zeng, Enhanced $H_2S$ sensor based on electrospun mesoporous $SnO_2$ nanotubes, J. Mater. Sci: Mater Electron 26 (2015) 9152–9157.

[40] W.H. Peng, C.L. Zhu, S.M Zhu, F. Yao, Y. Li, D. Zhang, Biomimetic fabrication of a-$Fe_2O_3$ with hierarchical structures as $H_2S$ Sensor, J. Mater. Sci. 48 (2013) 4336–4344.

[41] V. Balouria, A. Kumar , S. Samanta, A. Singh, A.K. Debnath, A. Mahajan,R.K. Bedi, D.K. Aswal, S.K. Gupta, Nano-crystalline $Fe_2O_3$ thin films for ppm level detection of $H_2S$, Sens. Actuators B: Chem 181 (2013) 471–478.

[42] Y. Wang, Y.M. Wang, J.L. Cao, F.H. Kong, H.J. Xia,J. Zhang, B.L. Zhu, S.R Wang, S.H. Wu, Low-temperature $H_2S$ sensors based on Ag-doped α-$Fe_2O_3$ nanoparticles, Sens. Actuators B: Chem 131 (2008) 183–189.

[43] V. Balouria, N.S. Ramgir, A. Singh, A.K. Debnath, A. Mahajan, R.K. Bedi, D.K. Aswal, S.K. Gupta, Enhanced $H_2S$ sensing characteristics of Au modified $Fe_2O_3$ thin films, Sens. Actuators B: Chem 219 (2015) 125–132.

[44] J. Kim, K. Yong, Mechanism study of ZnO nanorod-bundle sensors for $H_2S$ gas sensing, J. Phys. Chem. C 115 (2011)7218–7224.

[45] Z. Wen, L.P. Zhu, Y.G. Li, Z.Y. Zhang, Z.Z. Ye, Mesoporous $Co_3O_4$ nanoneedle arrays for high-performance gas sensor, Sens. Actuators B: Chem 203 (2014) 873–879.

[46] S.J. Chang, T.J. Hsueh, I.C. Chen, B.R. Huang, Highly sensitive ZnO nanowire CO sensors with the adsorption of Au nanoparticles, Nanotechnology 19 (2008) 17550.

[47] J.Y. Li, S.L. Xiong, B.J. Xi, X.G. Li, Y.T. Qian, Synthesis of CuO Perpendicularly Cross-Bedded Microstructure via a Precursor-Based Route, Cryst. Growth. Des. 9 (2009) 4108–4115.

[48] S.C. Zhang, Y.W. Huang, Z. Kuang, S.Y. Wang, W.L. Song, D.Y. Ao, W. Liu, Z.J. Li, Solvothermal Synthesized $In_2O_3$ Nanoparticles for ppb Level $H_2S$ Detection, Nanosci. Nanotech. Lett. 7 (2015) 455–461.

[49] Y. Wang, S. Wang, Y. Zhao, B. Zhu, F. Kong, D. Wang, S. Wu, W. Huang, S. Zhang, $H_2S$ sensing characteristics of Pt-doped -$Fe_2O_3$ thick film sensors, Sens. Actuators B: Chem. (2007) 79–84.